Electronic structure, stability, and mechanism of the decohesion and shear of interfaces in superhard nanocomposites and heterostructures

Electronic structure, stability, and mechanism of the decohesion and shear of interfaces in superhard nanocomposites and heterostructures

R. F. Zhang,[1] A. S. Argon,[2] and S. Veprek[1,*]
[1]*Department of Chemistry, Technical University Munich, Lichtenbergstrasse 4, D-85747 Garching, Germany*
[2]*Department of Mechanical Engineering, Massachusetts Institute of Technology, 77 Massachusetts Avenue, Cambridge, Massachusetts 02139, USA*
(Received 23 December 2008; revised manuscript received 19 May 2009; published 23 June 2009)

Electronic structure of interfaces, their stability and the mechanism of decohesion in tension as well as of ideal shear have been studied by means of *ab initio* density-functional theory for heterostructures consisting of a few nanometer thick fcc(NaCl)-TiN slabs with one monolayer of pseudomorphic SiN interface. It is found that the SiN interface sandwiched between fcc(001)-TiN slabs is unstable in its symmetric fcc structure, but it stabilizes by distortion of the Si-N bonds, which lowers the symmetry. Significant strengthening of the SiN interface occurs due to partial transfer of valence charge to the Si containing interface which induces damped valence charge-density oscillations propagating into the TiN bulk. As a consequence of these oscillations, decohesion, and ideal shear does not occur within the SiN interface, but in the TiN slabs between the Ti-N planes parallel to that interface. We provide a detailed study of this mechanism of decohesion and ideal shear on the atomic scale. The results are discussed in the context of the experimentally found hardness enhancement in heterostructures and superhard nanocomposites.

DOI: 10.1103/PhysRevB.79.245426 PACS number(s): 62.25.−g, 31.15.A−, 62.20.Qp, 73.22.−f

I. INTRODUCTION

Superhard nanocomposites consisting of 3–4 nm size nanocrystals of a hard transition-metal (Tm) nitride [TiN, VN, $(Ti_{1-x}Al_x)N$, $(Cr_{1-x}Al_x)N$…] "glued" together by about one monolayer (1 ML) thick covalent nitrides (e.g., Si_3N_4) with hardness ranging from 45 to ≥100 GPa, which were developed during the last decade,[1–3] attracted much attention of the scientific community and found also many industrial applications as protective coatings on tools for machining, such as drilling, turning, milling, stamping, forming and like.[4] Their nanostructure provides them with a large hardness enhancement by a factor of 3 to ≥5 as compared with the hardness of individual phases. The nc-TiN/a-Si_3N_4 nanocomposites (for the meaning of the symbols see Ref. 5) were studied in great detail and, therefore, represent the "prototype" system. For these reasons the focus in the present paper will be on this material. Because the experimentally obtained hardness enhancement and other properties of all nc-TmN/a-Si_3N_4 superhard nanocomposites, that were prepared according to the generic design principle,[1,3] show close similarities, the results of the present paper should be of general nature and applicable also to these systems.

We use *ab initio* density-functional theory (DFT) calculations in order to provide a detailed study of the electronic structure of the fcc(NaCl)-TiN/1 ML-SiN_x/TiN (see remark Ref. 6) interface and of the mechanism of decohesion and shear under applied load. Earlier experimental studies and the detrimental role of oxygen impurities on the mechanical properties were summarized in recent reviews and papers[3,7,8] to which we refer for further details. Here we shall mention only those results of the experimental work which are relevant to the present study.

When Argon and Veprek calculated, on the basis of measured indentation curves, that the tensile stress, which the ultrahard nc-TiN/a-Si_3N_4/$TiSi_2$ nanocomposites sustain without fracture, reaches values of ≥40 GPa, they concluded that the strength of these nanocomposites approaches the ideal strength of strong, flaw-free materials.[9–11] Thus, the about 1 ML thick Si_3N_4-like interface between the TiN nanocrystals[1,3] should be essentially free of flaws, i.e., there had to be an almost perfect binding between the silicon and nitrogen atoms in that interface, giving the same chemical shift of the Si 2*p* signal in x-ray photoelectron spectra, like in stoichiometric Si_3N_4, but with some strain due to mismatch of the sizes of the Si and Ti atoms (see Fig. 12b in Ref. 3). A 1 ML thick SiN_x interface in nanocomposites with randomly oriented TiN nanocrystals appears amorphous in x-ray diffraction (XRD) (Refs. 1 and 3) and selected area electron diffraction.[12]

The fcc(NaCl)-SiN 1–3 ML thin interface, pseudomorphically stabilized between several nm thick TiN layers, has been recently reported in TiN/SiN/TiN heterostructures deposited by reactive sputtering,[13–16] and it has been suggested to be the prototype of the interface in the "Ti-Si-N nanocomposites."[17] However, a variety of different (hkl) interfaces, possibly also faceted, have to coexist in superhard nanocomposites deposited at sufficiently high pressure of nitrogen and temperature. These must have randomly oriented TiN nanocrystals, fully segregated, stable Si_3N_4-like interfaces and show perfect stability up to ≥1100 °C without any internal friction signal.[3,18] Because the coatings reported in Ref. 17 were deposited at much lower temperature (see Refs. 17 and 19) than those reported in our papers,[1–3,20] they had a pronounced columnar structure and strong preferential orientation of the relatively large (≥10 nm) TiN crystals, as seen in Figs. 1 and 3 of Ref. 17. This is a significant difference when compared to the perfectly isotropic morphology with random orientation of 3–4 nm size nanocrystals in nanocomposites deposited by plasma chemical vapor deposition at 550 °C (Refs. 3, 12, and 20) or by reactive sputtering in pure nitrogen at 600 °C.[21] Furthermore, neither Kong *et al.* nor

Söderberg *et al.* have investigated if their "nanocomposites" and heterostructures remain stable upon annealing in nitrogen up to $\geq 1100\ ^\circ C$, as it has been demonstrated for the nanocomposites prepared according to the generic design principle.[1–3,18,20,22]

We emphasize that fcc(NaCl)-like-SiN may exist only as pseudomorphically stabilized 1–3 ML thick interfacial layers in the heterostructures. It collapses and becomes amorphous at a greater thickness.[13–15] This is due to the inherent instability of this material as shown by *ab initio* DFT calculations[23] and by more recent calculations of the phonon-dispersion curves.[24] Furthermore, the thermodynamic studies[25–27] showed that the Gibbs free energy of the reaction $3SiN+0.5N_2=Si_3N_4$, which corresponds to a sufficiently large activity of nitrogen, is -168 kJ/mol atom (see also remark Ref. 28). This is a large thermodynamic force driving the system toward stoichiometric, immiscible TiN and Si_3N_4 when a sufficiently high nitrogen pressure is used during the deposition, and a sufficiently high temperature is maintained in order to allow the system to complete the phase segregation by diffusion.[1–3,25]

It has been found in several nc-TmN/a-Si_3N_4 superhard nanocomposite systems that, when the crystallite size reaches a minimum value of about 3 nm, the hardness reaches a maximum.[1,3,20,29] Therefore, it has been suggested that there should be some strengthening resulting from the roughly 1 ML-Si_3N_4 interface because a minimum crystallite size means a maximum interfacial area per unit volume.[20] This prediction of strengthening has been recently confirmed by *ab initio* DFT calculations of Hao *et al.* for a fcc-TiN-$(111)/Si_3N_4-(10\bar{1}0)$ interface[30,31] and by Zhang *et al.* for several TiN/1 ML-SiN/TiN interfaces in both the fcc-TiN-like structure with octahedral coordination of Si to N as well as for the β-Si_3N_4-like structure with tetrahedrally bonded Si.[23,32] Similar strengthening has been recently reported also by Liu *et al.* for Si atoms inserted either interstitially or substitutionally into TiN with the strongest configuration being Si atom tetrahedrally coordinated to four N and four Ti atoms with Si-N bonds being significantly shorter than the Si-Ti distances.[33]

Hao *et al.* have shown that the 1 ML Si_3N_4 interface is the strongest configuration with a decohesion strength larger than that of bulk Si_3N_4 crystal. Similar strengthening by a factor of 4–10 as compared to the bulk fcc(NaCl)-SiN has been found for the 1 ML SiN interface by Zhang *et al.*, for both decohesion (which is relevant for brittle fracture) and shear (which is relevant for plastic deformation) in several significant crystallographic directions and slip systems.[23,32] In both cases the strengthening has been attributed to an enhanced valence charge density (VCD) at that interface. However, Hao *et al.* assumed that the SiN_x interface is the load carrier by fixing the relative position of Ti and N atoms in the upper and lower layers of the modeled slabs. Zhang *et al.* did not investigate the detailed electronic and atomic mechanism of decohesion and ideal shear. In view of the weak mechanical nature of the thermodynamically instable fcc(NaCl)-SiN (Ref. 23) one would intuitively assume that the 1 ML pseudomorphic SiN is also the weakest link in the heterostructures and nanocomposites, particularly when considering the recent work of Alling *et al.* who have shown on the basis of phonon-dispersion relations calculated by *ab initio* DFT that the bulk fcc(NaCl)-SiN is inherently, dynamically instable.[24]

In this paper we shall present an *ab initio* DFT study of the electronic structure and detailed electronic and atomistic mechanism of decohesion and shear of the fcc(NaCl)-SiN-like interfaces. It will be shown that the partial valence charge transfer to this interface actually increases its strength but also causes oscillations of the VCD between the Ti-N planes attached to it, which are damped with increasing distance. These oscillations cause that decohesion and ideal shear do not occur within the SiN interface, but between Ti-N planes adjacent to it.

II. COMPUTATIONAL METHOD USED

The *ab initio* DFT calculations were done using the "Vienna *ab initio* simulation package" (VASP) code[34–36] with the projector augmented wave method employed to describe the electron-ion interaction[37] and the generalized-gradient approximation for the exchange-correlation term[38] together with the Vosko-Wilk-Nusair interpolation. The integration in the Brillouin zone has been done on special k points of $9\times9\times9$ grids for the phases under consideration, and $5\times5\times3$ grids for the interface systems, determined according to the Monkhorst-Pack scheme,[39] energy cutoff of 600 eV, and the tetrahedron method with Blöchl corrections for the energy calculation and Gaussian smearing for the stress calculations, respectively. The conjugate gradient method has been used for the relaxation of structural parameters. The stress-strain relationships were calculated by incrementally deforming the model cell in the direction of the applied strain, and simultaneously relaxing the cell basis vectors conjugated to the applied strain, as well as the positions of atoms inside the cell, at each step. To ensure that the strain path is continuous, the starting position at each strain step has been taken from the relaxed coordinates of the previous strain step. This approach with a relaxed loading path has been successfully applied to the calculation of the strength of several strong solids recently.[40,41]

In order to check the reliability of our calculations, the equilibrium volume (V_0), the bulk modulus (B_0), and its pressure derivative (B_0') were determined by least square fit of the E-V curves (total energy vs volume) calculated by the *ab initio* DFT to three equations of state: The traditional Murnaghan equation,[42] those by Birch[43] and by Vinet.[44] The values of V_0, B_0, and B_0' obtained for the fcc(NaCl)-TiN and hcp(β)-Si_3N_4 are in good agreement with experimental results and calculated values reported in the literature.[26] The calculated values of the hypothetical fcc(NaCl)-SiN, which has been observed only as heteroepitaxially stabilized 1–2 ML thick interface in TiN/SiN/TiN heterostructures,[13–16] could not be compared with experimental data. Nevertheless, our calculated value of the first derivative of the bulk modulus, B_0', of this phase of about 4 is within the range predicted by the universal binding-energy relation.[45] The value of the bulk modulus of hcp(β)-Si_3N_4 is about 27% higher than that of fcc(NaCl)-SiN indicating a smaller strength of the latter.[26]

TABLE I. Changes in the total energy as result of displacement of Si atoms by 3% in the three relevant directions x, y, and xy, which are within the Si plane, and z, which is perpendicular to it. Notice that the more negative the total energy the more stable that configuration is. Unit is eV/supercell.

Displacement of Si atoms		$\delta=0\%$	$\delta_x=3\%$	$\delta_y=3\%$	$\delta_x=\delta_y=3\%$	$\delta_z=3\%$
E_{tot} (eV)	(001)	−150.179096	−150.192595	−150.192594	−150.203441	−145.343269
	(111)	−170.067276	−170.046805	−170.046880	−170.046779	−166.341201
	(110)	−228.329255	−228.325519	−228.302938	−228.300169	−225.971418

For convenience, all the Miller indices for interfaces in the following text are marked with respect to the unit cell of fcc(NaCl)-TiN.

During the calculations of the stress-strain dependences, the stress reaches a maximum (corresponding to the ideal strength for the given mode of deformation) at a relatively large strain, which may significantly change the crystal symmetry and the electronic structure. Therefore, we checked for any difference in the results of the calculations of the stress-strain curves for different meshes of k points. We obtained essentially the same results by choosing a larger mesh of $10\times10\times10$ k points as compared to $9\times9\times9$ for bulk phases. A similar check has been done also for the interfaces. For example, the calculated peak normal stress just before lattice instability (i.e., close to the ideal decohesion strength) of the (001) interface is 25.99 GPa with $5\times5\times3$ k points and 25.63 GPa with $7\times7\times5$ k points at the same normal strain of 0.1576 with a strain step of 0.05. For the (111) interface, the calculated peak normal stress is 56.8 GPa with $5\times5\times3$ k points and 57.9 GPa with $7\times7\times5$ k points at the same strain of 0.1576. As a further verification, we tested a possible effect of the cell size used in the calculations. For the same tensile strain of 0.1576 (just before the instability) the calculated peak normal stress on the (001) interface of about 26.1 GPa for the larger cell containing 32 atoms compares well with the values of 25.99 GPa for the smaller cell of 16 atoms. Also for the (111) interface, the calculated peak normal stress of 39.99 GPa for the larger cell (36 atoms) compares well with the value of 39.77 GPa for the smaller one (18 atoms) at the same normal strain of 0.1025, and the lattice instability occurs at the same critical strain of 0.15 and similar peak normal stress for both cells. These extensive checks of our procedure support the reliability of our *ab initio* DFT calculations for both bulk phases and interfaces.

III. RESULTS

A. Stability of the relaxed interfaces

As mentioned above, the substoichiometric fcc(NaCl)-SiN is thermodynamically unstable with respect to hcp(β)-Si_3N_4, and the lattice of the pseudomorphically stabilized interface in the TiN/SiN/TiN heterostructures collapses when its thickness exceeds a few monolayers. Moreover, some of the stress-strain curves calculated by means of *ab initio* DFT in Refs. 23 and 32 showed concave shape at small strains indicating that there should be a (local) maximum of the total energy at zero strain, i.e., the related interfaces should be inherently unstable. Therefore, in the present paper, we first studied the (local) stability of the relevant pseudomorphic interfaces in the following way:

Using the *ab initio* DFT calculation we first fully relaxed the "input" cell (i.e., TiN in which the central layer of Ti has been replaced by Si) to minimum total energy without any applied stress. Because the VASP code keeps constant the given symmetry of the cell during this relaxation, this "minimum total energy" does not ascertain a local minimum of the system with respect to finite displacements. Therefore, we have, as a subsequent step, calculated the changes of the total energy when imposing small, finite displacements to the silicon atoms in the x and y directions, within the Si-plane, and the z direction perpendicular to it. The results are shown in Table I for a displacement of 3%, which was chosen for the initial test of the stability. Considering that in our notation, the more negative the total energy the more stable is that configuration, one can see that the (001) interface is unstable against displacement in the x, y, and xy, i.e., [110], [$1\bar{1}0$], and [100] directions, respectively, but stable against displacement in the z direction. However, the (111) and (110) interfaces are (locally) stable.

The silicon atoms with six nitrogen neighbors are "overcoordinated" in the fcc(NaCl)-SiN, because its "natural" coordination derived from four valence electrons in $2s$ and $2p$ orbitals is four. The sixfold coordination is known only in some nitridosilicates, such as $C_{16}Si_{15}O_6N_{32}$ (Ref. 46) or high-pressure phases, such as the Stishovit phase of silica and the spinel phases of the fourth group elements, such as γ-Si_3N_4, γ-Ge_3N_4, γ-$(Si_{1-x}Ge_x)_3N_4$ and γ-Sn_3N_4.[47,48] The spinel structure consists of 8 f.u. of a total of 56 atoms of which eight cations (Si, Ge, Sn) are in tetrahedral (fourfold coordinated to N) and 16 in octahedral (sixfold coordinated to N) sites, whereas nitrogen is fourfold coordinated to the cations. In the past, a higher coordination number of silicon in some organosilicon compounds has been attributed to the participation of the $3d$ orbitals in the hybridization with $2s$ and $2p$,[49] but more recently this concept has been questioned by several authors (see Ref. 50 for a review). Obviously, there is no stable compound where all Si atoms would be sixfold coordinated to nitrogen only, as in the fcc(NaCl)-SiN.

Therefore we conclude that, from the chemical point of view, bulk fcc(NaCl)-SiN is an intrinsically unstable compound, in agreement with the recent phonon-dispersion study of Alling *et al.*,[24] and also 1 ML "fcc(NaCl)-SiN" (001) interface with full fcc symmetry is unstable. However, one may ask if the 1 ML—(001) SiN interface may be stabilized by decreasing its symmetry, because there are many examples where highly symmetric configurations in molecules and crystals, particularly those with a high coordination

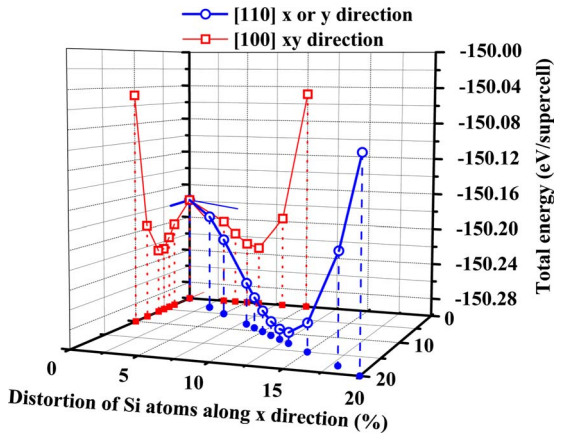

FIG. 1. (Color online) Dependence of the total energy (eV/supercell) on the displacement of Si atoms within the (001) interface as indicated in the inset.

number, decrease their energy by decreasing their symmetry: e.g., Jahn-Teller distortion, lowering of the symmetry to a noncentric space group in ferroelectrics below the Curie temperature, the split interstitial effect in fcc metals, inert pair effect, and the like.[51]

In order to answer the question regarding the possible instability of the 1 ML (001) interface, we calculated the dependence of the total energy of the cell on the finite displacement of Si atoms in the x, y [110] and xy [100] directions in that interface. Figure 1 shows that there is a local energy minimum at a displacement of $\pm 6\%$ for the displacement in the xy direction, and at a displacement of $\pm 12\%$ for the x or y displacements. Because the minimum in the x or y direction is deeper than those into the xy ones, the latter are saddle points with respect to the minimum in the x or y direction. The cell after full relaxation, and after the displacement of the Si atoms into the local minimum of total energy, is shown in Figs. 2(a) and 2(b), respectively. Figures 2(c) and 2(d) are the corresponding top views and Figs. 2(e) and 2(f) show the corresponding arrangement of Si to N neighbors. Obviously, the arrangement of the 1 ML Si after the cell relaxation corresponds to a tetragonal-like symmetry which is lower than that of the fcc one. However, after the x or y displacement of Si atoms by 12% into the deeper local minimum of the total energy (Fig. 1), the symmetry is strongly lowered as seen in Figs. 2(d) and 2(f). The Si-N distance of 0.2522 nm to the atoms on the left-hand side in Fig. 2(f) is too large to be assigned to a covalent bond (notice, that bond length in the bulk, unstable fcc(NaCl)-SiN crystal is 0.2131 nm and in the stable, stoichiometric, hcp(β)-Si_3N_4 0.1764 nm). Obviously, the silicon atoms are trying to arrange into a kind of fourfold coordination to the two N atoms on the right and on the top and bottom.

One notices that the displacement of the Si atoms is seen only when viewing in the [1$\bar{1}$0] direction [perpendicular to the plane of Fig. 2(b)] but not when viewed in the [110] direction (i.e., from the left to right in that figure). Because of this fact and in view of the relatively small value of the displacement, it is difficult to recognize it even in high-quality, high-resolution transmission electron micrographs

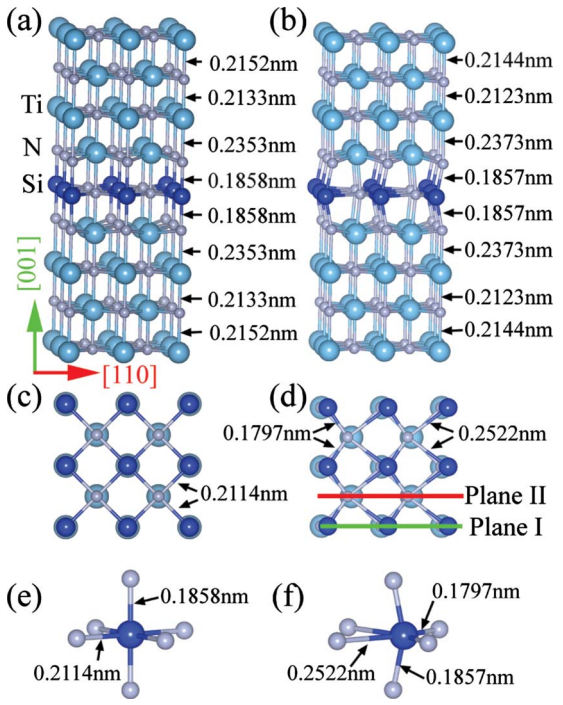

FIG. 2. (Color online) The (001) interfaces after full relaxation (a) with Si atoms located in high-symmetry octahedral positions and (b) after the displacement of the Si atoms into the minimum of total energy for the x or y movement shown in Fig. 1. The numbers give the interatomic distances. Figures 2(c) and 2(d) are the corresponding top views which show the shortened and elongated Si-N bonds, and Figs. 2(e) and 2(f) show the corresponding arrangement of Si to N first neighbors. The top view in Fig. 2(d) assigns plane I which contains Si atoms within the interface and plane II which contains only Ti and N atoms. Dark (blue) atoms are Si, small light (blue) atoms are N, and larger light (blue) atoms are Ti.

(HRTEM) presented by Söderberg *et al.*[13,14] Thus we conclude, that the (001) interface, which is inherently unstable in its symmetric, octahedral-like structure, reduces its energy to a local (metastable) minimum by strongly decreasing its symmetry when forming the configuration shown in Fig. 2(f).

A close look on Fig. 2(b) shows that there are oscillations of the interplanar distances whose amplitude decays with increasing distance from the interface. These are due to oscillations of VCD, first identified as such by Friedel[52–54] which we discuss in the next section. Friedel oscillations occur, e.g., at the abrupt interface between a crystal and vacuum, liquid and solid, in semiconductors and metals as results of charged impurities, and they are also observed in a variety of other phenomena in nanosized materials.[52–54] Here we shall first complete the discussion of the structure of the relaxed (111) and (110) interfaces which are in (local) energy minima (Table I). Figure 3 shows the (111) and (110) cells with 1 ML Si interface. One notices that also in this case the fcc symmetry is reduced by a distortion of the interatomic distances. Interestingly, the reduction in the symmetry, as compared with the undistorted cell, is smaller in these cases than in the (001) interface, and these relaxed configurations are (locally) stable (Table I). A study of the detailed reasons

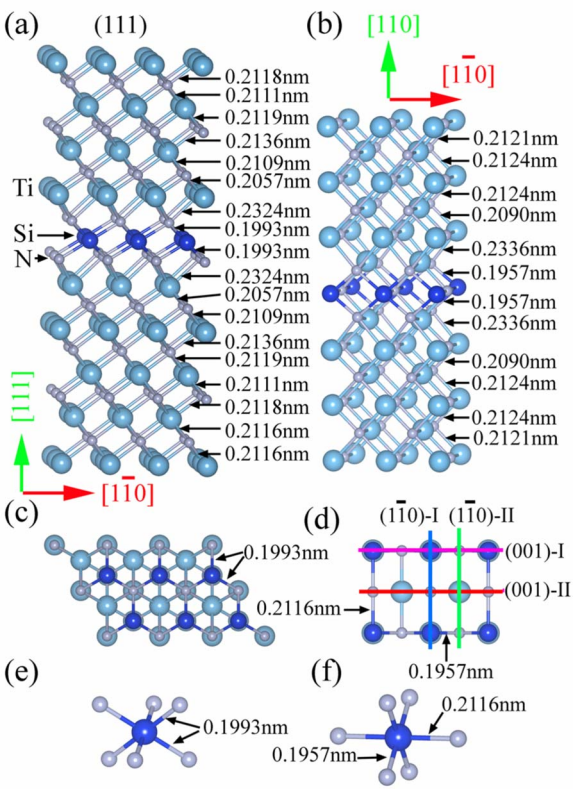

FIG. 3. (Color online) The (a) (111) and (b) (110) interface after full relaxation. The numbers in the figures are the interatomic distances. Figures 3(c) and 3(d) are the corresponding top views which show the Si-N bond distances, and Figs. 3(e) and 3(f) show the corresponding arrangement of Si to N first neighbors. The top view in Fig. 3(d) assigns four types of planes (001)-I, (001)-II, (1$\bar{1}$0)-I, and (1$\bar{1}$0)-II which will be discussed later.

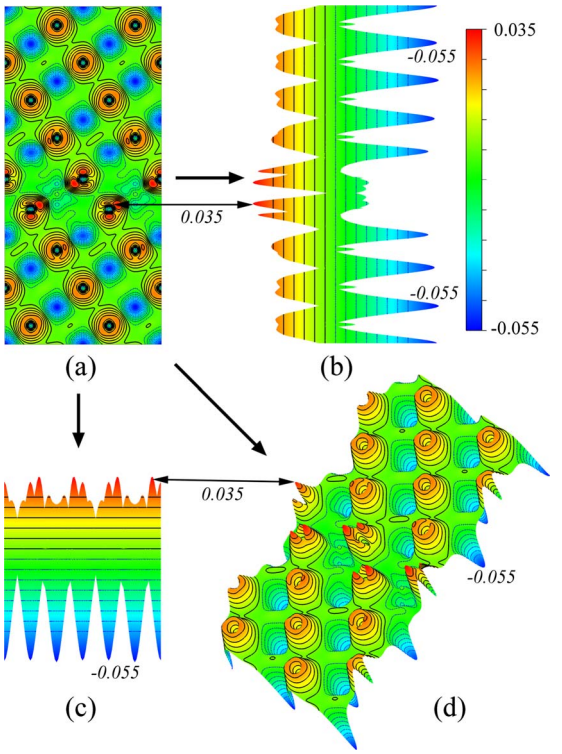

FIG. 4. (Color online) (a) Valence charge-density difference of the TiN(111)/1 ML-SiN/TiN(111) interface, and the corresponding bird's eye view profile seen from different directions marked by arrows: (b) left view and (c) top view, and (d) side view. The color scale runs from −0.055 at bottom blue to 0.035 electrons/Bohr^3 at top red. The small (black) italic numbers indicate the values of the VCD.

for this finding, albeit interesting, is beyond the scope of the present paper. We just emphasize that, as seen in the top two figures (a) and (b) of Fig. 3, Friedel oscillations occur also in these cells. It should be mentioned, that also Hao *et al.*[30,31] found similar oscillations of the bond distances in his calculations of the TiN-Si_3N_4 system using a different DFT code. At that time, Hao *et al.* have been interested in the strengthening of the Si_3N_4-like interface (see below) and did not realize the meaning of these oscillations. Therefore, these researchers did not study the effect of the Friedel oscillations in more detail.

B. Valence charge-density difference and Friedel oscillations

A close look on Figs. 2 and 3 shows that the Si-N bonds directed out of the 1 ML Si interface are shorter than those in bulk fcc(NaCl)-SiN crystal (0.2131 nm), and the shortest bonds in the strongly deformed (001) interface of 0.1797 nm is comparable with that in the stable, stoichiometric, bulk hcp(β)-Si_3N_4 (0.1764 nm). This is indicative of the strengthening of that interface as reported in our previous paper[32] and also by Hao *et al.* for the semicoherent TiN-(111)/1 ML-Si_3N_4−(10$\bar{1}$0) interface.[30,31] The Ti-N bond length in the layer next to the SiN interface has the longest bond distance of 0.2373 nm for the (locally) stable (001) interface, of 0.2324 nm for the (111), and of 0.2336 nm for the (110) interface. These values are larger than that calculated for fcc(NaCl)-TiN of 0.21285 nm. With increasing distance from the SiN interface, the Ti-N bond lengths show damped oscillations approaching the equilibrium value. The Friedel oscillations of the VCD, as seen also in the variable bond distance, reflect the oscillatory nature of VCD in TiN near the SiN interface, because due to the larger electronegativity of Si (1.8) as compared with Ti (1.5) (Ref. 55) and the formation of strong covalent Si-N bonds, the interface is negatively charged.

The origin of the damped oscillations of the bond distances are the oscillations of the VCD, which will be used to study the details of the decohesion and ideal shear across interplanar gaps next to the interfaces. However, more illustrative and easily visible for the reader are the oscillations of valence charge-density differences (VCDD) defined as the difference between the calculated VCD of the system and those of neutral atoms at the given position. An example of VCDD for the (111) interface is shown in Fig. 4. A positive value (red color and thicker solid contours) means an increase in the negative charge while a negative value (blue color and thinner dotted contours) means a decrease, as compared to the neutral atoms. Thus positive and negative values of VCDD reflect stronger and weaker interatomic bonds, respectively.) The VCDD maps shown in Fig. 4 provide an

illustrative picture of the strengthening of the SiN interface, the weakening of the Ti-N layer next to the interface, and of the associated Friedel oscillation. We do not show here the (001) and (110) interfaces because they do not involve any significantly new physical picture.

In our previous paper we have shown that the ideal tensile decohesion as well as shear strengths are enhanced by a factor of ≥ 4 as compared to bulk fcc(NaCl)-SiN which is a weak, instable nitride.[32] However, all these values of ideal strengths were lower than those of bulk TiN. This is obviously due to the weakening of the Ti-N layer next to the SiN interface. Hao *et al.*[30,31] also reported enhancement of decohesion strength of the fcc-TiN-$(111)/Si_3N_4-(10\bar{1}0)$ interface as compared with bulk Si_3N_4. These researchers could not see the weakening of the Ti-N interplanar bonds next to the SiN interface because they performed the computational decohesion "experiment" by fixing the relative positions of the Ti and N atoms in the upper and lower TiN slabs. In such a way they were able to determine the decohesion strength of the Si_3N_4 interface but not that of the neighboring TiN bonds. Nevertheless, they also observed the oscillations of the bond distances[30,31,56] reflecting the presence of Friedel oscillations. Liu *et al.* have also observed a shortening of the Si-N bonds and elongation of the Ti-N ones[33] which suggests the presence of Friedel oscillations also in their case. Therefore, the effects of the Friedel oscillations on the mechanism of decohesion and ideal shear of the (111) interface, which have been described in our previous paper,[57] and on of the (001) and (110) interfaces to be discussed here, are possibly of general nature for other interfaces in TiN/SiN_x, and in other TmN/SiN_x nanocomposites and heterostructures.

Because the (111) interface contains only Si atoms and all atomic layers parallel to it contain only one sort of atoms (either N or Ti), we note that the Friedel oscillations, in the sense of displacements along the neighboring atomic planes perpendicular to the interface, are "in phase" around this interface.[57] However, in the cells with the SiN interfaces parallel to the (001) and (110) planes of TiN, the SiN interface, and the planes parallel to those interfaces always contain two sorts of atoms (Si and N in the interface, and Ti and N in the TiN layers within TiN away from both sides of the interface). This results in a kind of "phase shift" of the Friedel oscillations between the neighbor atomic planes perpendicular to the interface, which contains only Si or N within that interface. This can be clearly seen on the (001) interface shown in Fig. 2(b): the Si-N bond distances perpendicular to the (001) interface are clearly shorter than the N-Ti ones coming out of the SiN interface, and this feature is seen to propagate also in the subsequent layers parallel to that interface.

We shall see that these phase shifts of the Friedel oscillations have important consequences on the sequence of bond ruptures in the terminal responses of decohesion and bond flip over, rotation, and rearrangement in ideal shear. For these reasons, we shall present in the following sections a detailed study of the deformation and failure of the TiN/1 ML-SiN/TiN sandwich for the (001) and (110) interfaces under a variety of loading. In order to save space in this paper, we shall restrict our discussion to only several illustrative examples of decohesion and ideal shear which demonstrate the essential features.

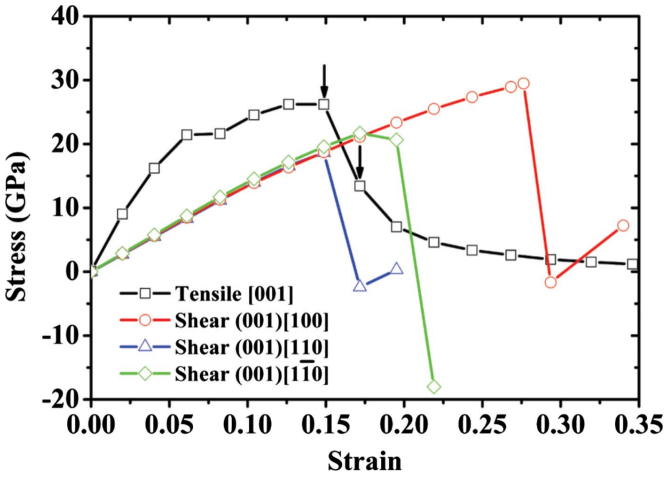

FIG. 5. (Color online) Calculated stress-strain curves for the stable TiN(001)/1 ML-SiN/TiN(001) interface [see Fig. 2(b)] and the deformation modes as indicated. The arrows indicate the points just before and after the instability in the case of tensile strain and stress applied in the [001] direction normal to that (001) plane. See remark in Ref. 58.

C. Valence charge density upon decohesion and ideal shear

1. (001) interface

Figure 5 shows the calculated stress-strain curves for the TiN(001)/1 ML-SiN/TiN(001) interface [c.f. Fig. 2(b)], loaded in tension perpendicular to the interface, and in shear for the three significant slip systems.[58] A comparison with the shear curves for $(001)[1\bar{1}0]$ and (001)[100] slip systems for the relaxed cell shown in Fig. 2(a) (see Fig. 6 in Ref. 32) with those of the (locally) stable interface in Fig. 2(b) (see Fig. 5) reveals that the latter interface has a somewhat lower ideal shear strength. In the following figures, we shall show the VCD just before and after the instability. For the convenience of the reader we illustrate these two points by arrows in Fig. 5 for the tensile strain applied along the [001] direction. In all other cases the reader can identify the points on the stress-strain curves in Fig. 5 according to the value of strain indicated in the figures with VCD.

Because of the "phase shifts" of the Friedel oscillations discussed above, we have to distinguish between the planes perpendicular to the interface which contain, within the SiN interface, only Si atoms from those which contain only N atoms. These are shown in Fig. 2(d) as plane I and plane II. One notices that the longest N-Ti bonds in plane I are those where the nitrogen is shared between Si and Ti, whereas in plane II, it is the N-Ti bond directly attached to nitrogen within the SiN interface. Thus, the oscillations of bond lengths in plane I and II are "phase shifted" with respect to each other.

The VCD during the applied tensile strain along the [001] direction normal to the (001) SiN interface is shown in Fig. 6 just before [Fig. 6(a)] and after [Fig. 6(b)] the instability of the stress-strain curve in Fig. 5. One can see that whereas the Si-N distance out of the interface differs only very little from that in equilibrium of 0.1857 nm [cf. Fig. 2(b)], the N-Ti interplanar bond in the layer next to the SiN carries almost

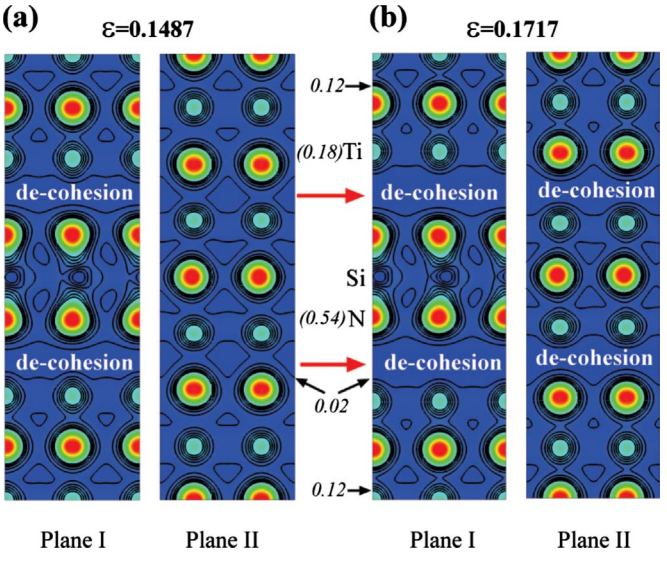

FIG. 6. (Color online) The changes in valence charge density of the stable TiN(001)/1 ML-SiN/(001)TiN interface during applied tensile strain to (001) distorted interfaces [see Fig. 2(b)] along the [001] direction normal to that interface: (a) just before (strain ε =0.1487) and (b) after (strain ε=0.1717) the instability. The small (black) italic numbers indicate the contours of the VCD.

the entire tensile strain, applied to the whole cell. Moreover, decohesion commences within the plane I, which contains the Si atoms in the interface, already before the instability of the stress-strain curve (see Fig. 5), whereas in plane II, which contains only N atoms within the SiN interface, the decohesion occurs only after the instability. The phase shift of the Friedel oscillations is responsible for this phenomenon.

There is obviously electronic interaction between the "more covalentlike" plane I and the "more metalliclike" plane II, which is responsible for the fairly smooth shape of the decohesion curve after the instability, where the processes in one plane drag those in the other along and where the stress decreases continuously to zero with increasing strain as a result. In contrast, the stress-strain curve for decohesion of the (111) interface, where the Friedel oscillations are in phase, shows an abrupt decrease just after the instability (see Fig. 2 in Ref. 57). We shall see later, that decohesion of the (110) interface is even more complex. Notice also that the Si-N distance of 0.1825 nm after the instability is shorter than that of 0.1857 nm in the equilibrium state at zero strain [c.f. Fig. 2(b)].

Figure 7 shows the VCD behavior upon shear stress applied across the (001) interface in the [110] direction, which is the weakest one (see Fig. 5). The white arrow shows the flip over of the Ti-N bond from atom Ti(1) to Ti(2) due to the shear displacement. One can see that in plane I the flip over occurs between the Ti and N which is bonded to Si, whereas in plane II it occurs between Ti bonded to N within the SiN interface. Thus, the shears in plane I and II occur "phase shifted" in a similar manner as the decohesion. The depletion of VCD within the "sliding Ti-N interface" in plane I is larger than that in plane II because the former contains Si atoms within the SiN interface which strongly attract valence charge from the N atoms adjacent to the "sliding Ti-N interface."

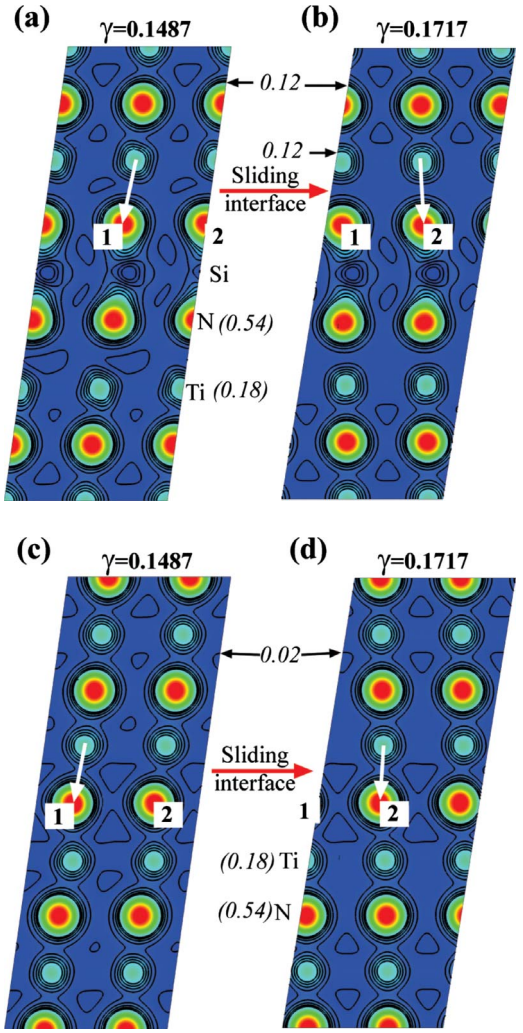

FIG. 7. (Color online) The changes in valence charge density of the stable TiN(001)/1 ML-SiN/(001)TiN interface during ideal shear just before (strain γ=0.1487) and after (strain γ=0.1717) the instability of the stress-strain curve (see Fig. 5) shown in Fig. 7(a) and Fig. 7(b) in plane I, and Fig. 7(c) and Fig. 7(d) in plane II for the distorted, stable (001) interfaces upon shear applied in the [110] direction. The white arrow shows the flip over of the Ti-N bond from atom N(1) to N(2) due to the shear. The small (black) italic numbers indicate the contours of the VCD.

Notice that after the instability, the system is still not fully relaxed. The negative value of the stress in Fig. 5 means that the system tries to restore the crystal symmetry to a new equilibrium by completing the shear displacement to one-atomic distance. This is even more pronounced for the (001)[1$\bar{1}$0] slip system (see Fig. 5). We note that the unloading portions of the shear curves in Fig. 5, past the point of maximum resistance, show a sharp drop rather than the expected smooth decline resembling the expected Frenkel sinusoid.[59] This is an artifact of elastic unloading in the upper and lower parts of the crystal outside the actual sheared zone while the shearing strain increases in the intense shearing zone. This is accentuated by the representation of the average shear strain across the cell, rather than just what occurs inside the intense shearing zone (see also Fig. 2.2 on

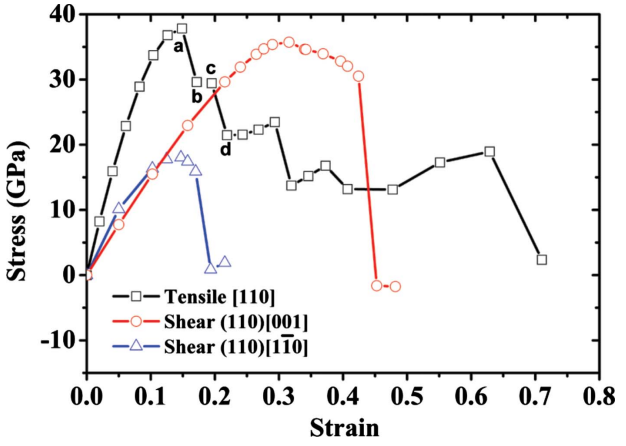

FIG. 8. (Color online) Calculated stress-strain curves of TiN(110)/1 ML-SiN/(110)TiN interface for the deformation modes as indicated. The letters inserted on the decohesion curve indicate the values of strain for which the VCD is shown in Fig. 11.

page 50 in Ref. 60). We did not calculate the whole curves because of the large computing time needed and because it would not provide any new physical insight. The behavior of the VCD during the shear in the other directions (see Fig. 5) is similar showing also the effect of the phase shift of the Friedel oscillation on the flip over of the Ti-N bonds. Therefore we do not show it here.

2. (110) interface

Figure 8 shows the stress-strain curves calculated for the TiN(110)/1 ML-SiN/TiN(110) interface (see remark Ref. 61). Letters a, b, c, and d in Fig. 8 indicate the strain values for which VCD evolution will be shown in Fig. 11 below. The value of the ideal decohesion strength is between those of the (001) and (111) interfaces whereas the ideal shear strength of the (110)[001] slip system is the highest of all. This is a direct result of the fact that the ideal shear strain of the (110)[001] system is larger by a factor of 2.83 than that of the (111)[110] system, as is clear from the NaCl type structure of TiN. This, by the simple Frenkel sinusoid model of ideal shear immediately accounts for the rather different shear resistances of these two ideal shear systems. Parenthetically, the shapes of these curves clearly differ from those for the (111) (Ref. 57) and (001) interfaces where no such corresponding large differences in the ideal shear responses were present:

(1) The shear curves show a maximum of stress followed by its smooth decrease before the final instability whereas those for the (111) and (001) reach a maximum just before the instability occurs.

(2) The curve for tensile load shows, after the instability, a step-wise behavior with several ranges where the stress slightly increases with increasing strain.

These phenomena are related to the complex changes in the electronic structure of this interface upon deformation. In order to illustrate this we show in Fig. 9 a more detailed view of the structure of this interface and of four atomic planes which will be important in the further discussion. This structure and values of the bond distances correspond to the state

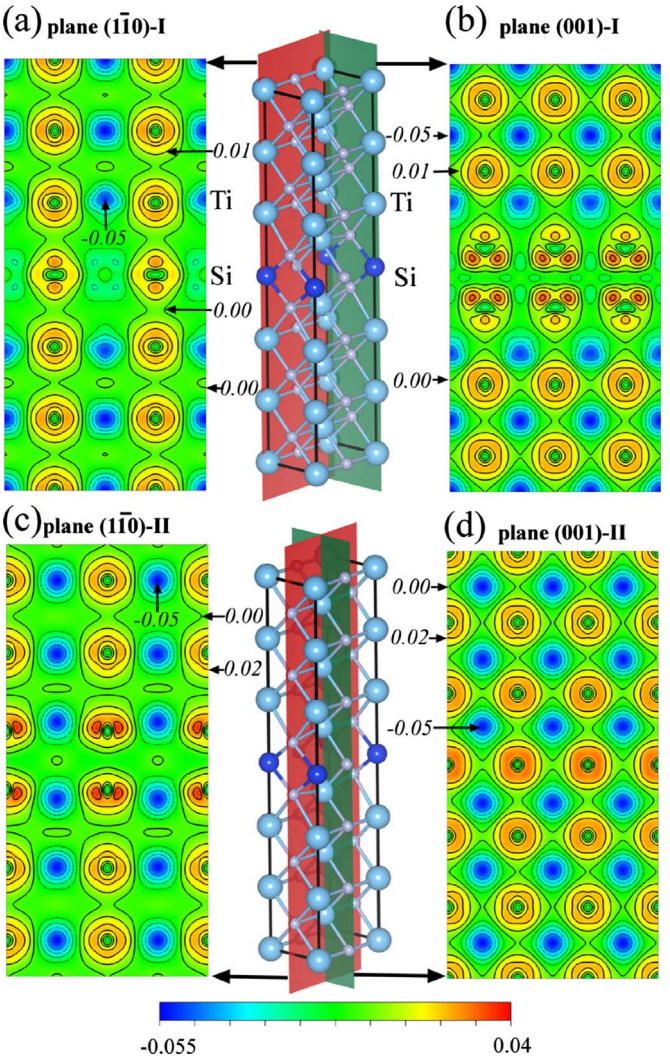

FIG. 9. (Color online) Valence charge-density difference in the plane I, which contains Si-atoms in the TiN(110)/1 ML-SiN/(110)TiN interface shown in the (a) (1$\bar{1}$0)-I, (b) (001)-I planes, (c) (1$\bar{1}$0)-II, and (d) (001)-II planes as illustrated in the middle of the figure. The color scale runs from −0.055 at bottom (blue) to +0.04 electrons/Bohr^3 at the top (red). The small (black) italic numbers indicate the contours of the VCDD.

after full relaxation of the total energy to the (locally) stable state as described above. By analogy to the above discussion of the (001) interface, planes I are perpendicular to the interface and contain Si atoms within the SiN interface, whereas planes II are running through the chains of N atoms in that interface. For both, planes I and II, we distinguish between planes (1$\bar{1}$0) and (001) as shown in the top view of Fig. 3(d). Like for the (001) interface, the Friedel oscillations show phase shift because the Si-N bonds extending out of the SiN interface in planes I are the shortest ones [0.1957 nm, see Fig. 3(b)] followed by the longest N-Ti ones (0.2336 nm), whereas in planes II the N-Ti bonds out of the SiN interface are with 0.2167 nm [see Fig. 3(a)] longer than the next following Ti-N bonds of 0.2079 nm. These differences are due to a higher electronegativity of Si as compared to Ti and the

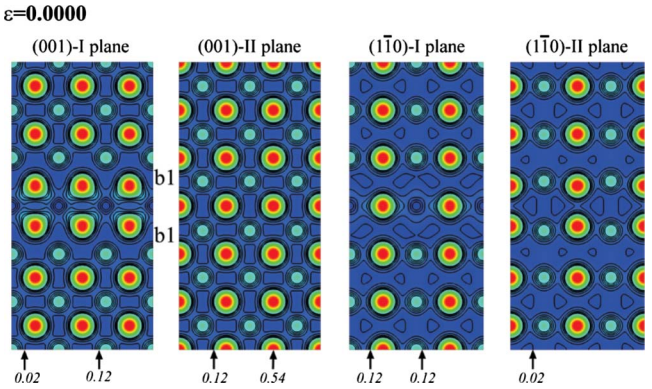

FIG. 10. (Color online) The valence charge density of the TiN(110)/1 ML-SiN/(110)TiN interface shown for the four relevant planes after full relaxation at zero strain. The small (black) italic numbers indicate the contours of the VCD.

formation of strong Si-N bonds that weaken the neighbor N-Ti ones.

Figures 9(a) and 9(b) show the VCDD in the planes I (1$\bar{1}$0) and (001), respectively, as illustrated in the middle of the figure and in the following denoted as (1$\bar{1}$0)-I and (001)-I. Figures 9(c) and 9(d) show the corresponding planes II (1$\bar{1}$0) and (001) which are further denoted as (1$\bar{1}$0)-II and (001)-II, respectively. Again, these figures correspond to the fully relaxed state at zero strain. For the sake of the discussion of the decohesion and ideal shear, we show in Fig. 10 the VCD maps of the TiN(110)/1 ML-SiN/(110)TiN interface for the four relevant planes after full relaxation at zero strain. One notice the large differences in the VCD in the four planes, which, as we shall see, play a role in the atomistic mechanism of decohesion and ideal shear. Again, the N-Ti bonds next to the SiN interface are the weakest ones, particularly in the (001)-I plane. One notices the very low VCD within the interplanar N-Ti bonds attached next to the SiN interface in the (001)-I plane (see "b1" in Fig. 10 left).

Figure 11 shows the changes of the VCD around the TiN(110)/1 ML-SiN/(110)TiN interface upon applied tensile strain along the [110] direction, which is perpendicular to the (110) SiN interface, for all four relevant planes specified in Fig. 3(d). The values of the applied strain, (a) 0.1487 just before the instability, and (b) 0.1717, (c) 0.1951, and (d) 0.2190 after the instability, are indicated in each figure and can be compared with those in Fig. 8. A comparison of Fig.

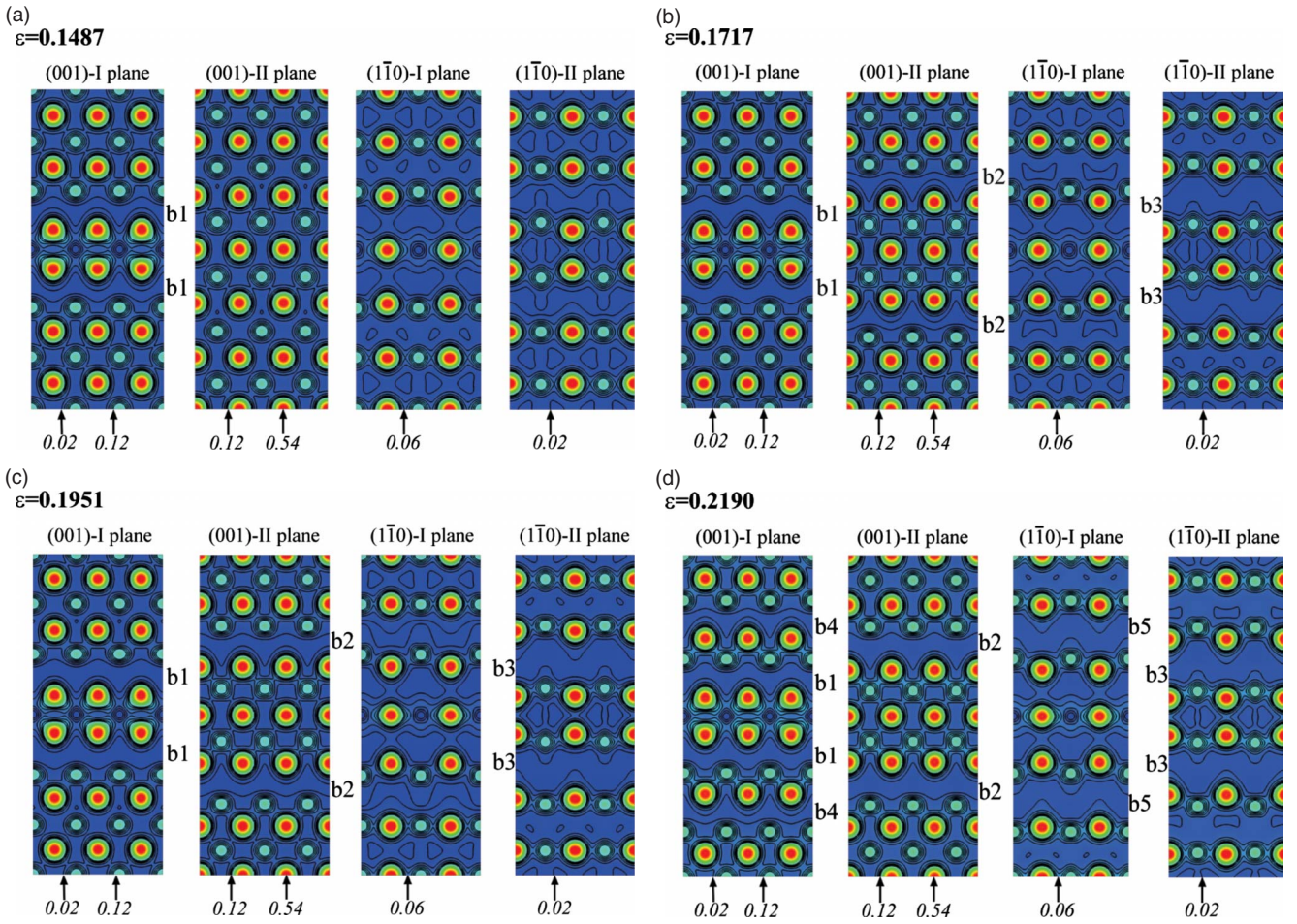

FIG. 11. (Color online) The changes in the valence charge density of the TiN(110)/1 ML-SiN/(110)TiN interface upon applied tensile strain along the [110] direction, which is perpendicular to the (110) SiN interface, for all four relevant planes specified in Fig. 3(d). The values of the applied strain are indicated in each figure and can be compared with those in Fig. 8. The small (black) italic numbers indicate the contours of the VCD.

11(a) for strain of 0.1487 just before the decohesion instability (see Fig. 8) with Fig. 10 shows a decrease in the VCD in the region b1 of the (001)-I plane, and smaller changes in the other ones. After the instability at strain 0.1717 [see Fig. 11(b)], VCD depletion indicative of the onset of decohesion is seen in regions marked b1, b2, and b3 in planes (001)-I, (001)-II and $(1\bar{1}0)$-II, respectively, but much less change in plane $(1\bar{1}0)$-I. Because the regions b1, b2, and b3 are in different interplanar N-Ti bonds located at different distance from the SiN interface, and the $(1\bar{1}0)$-I plane still withstands decohesion, the stress-strain curve (Fig. 8) somewhat "stabilizes" for the next strain step to the value of 0.1951 [see b and c of Fig. 8]. This "stabilization" is due to a partial transfer of the valence charge from the weakened bonds to the neighboring ones in a different distance from the SiN interface. Upon a further increase in the strain to the value of 0.2190, a decrease in the stress is seen in Fig. 8 (see point d), and new onsets of decohesions marked by b4 and b5 are seen in the VCD shown in Fig. 11(d). These bonds are located further from the SiN interface. Thus, the decohesion event is not localized to one layer parallel to the interface as found, e.g., for the (111) interface where the N-Ti bonds attached directly to the SiN interface break (see Fig. 3 in Ref. 57), but it spreads more into the interior of the TiN slab. The appearance of several discontinuities followed by a temporal stabilization, which are seen on the decohesion curve in Fig. 8, have their origin in similar restructuring and delocalization of the VCD distribution into the interior of the TiN slab. The latter is a consequence of the complex "phase shifts" of the Friedel oscillations within the atomic planes perpendicular to the interface.

Next we shall study the mechanism of the ideal shear within the slip systems shown in Fig. 8. Figure 12 shows the changes in the VCD of TiN(110)/1 ML-SiN/(110)TiN interface upon shear applied in the $[1\bar{1}0]$ direction just (a) before (strain γ=0.1700) and (b) after (strain γ=0.1934) instability in both (001)-I and (001)-II planes. Comparing with Fig. 10 one can see a slight rotation of the N atoms around the Si and Ti atoms within the planes (001)-I and (001)-II, respectively, as illustrated by the white arrows just before the instability at strain of 0.1700. This rotation is responsible for the slight decrease in the stress with increasing strain after the stress maximum at strain of about 0.15 (c.f. Fig. 8) because, although Si atoms are still bonded to four N neighbors in the plane, the distance to the N-atoms number 2 and 4 increases resulting in a "softening" of the interface. After the instability of the stress-strain curve at strain of 0.1934 (c.f. Fig. 8), these bonds break forming strong bonds with two up and down neighbor Si atoms, and the N atoms number 1 and 3 rotate clockwise as shown in Fig. 12(b). As a result, strong Si-N bonds in the direction perpendicular to the interface are formed [see the white lines in Fig. 12(b)], with a noticeable decrease in the VCD to the left and right from them, when the shear stress decreases to zero (c.f. Fig. 8). In the (001)-II plane, Ti atoms rotate around the N atoms which are within the SiN interface resulting also in Ti-N-Ti bonds arranged perpendicularly to the interface and VCD depletion to the left and right [c.f. Fig. 12(b) with Fig. 10]. This zero-stress state is a metastable intermediate because a new equilibrium

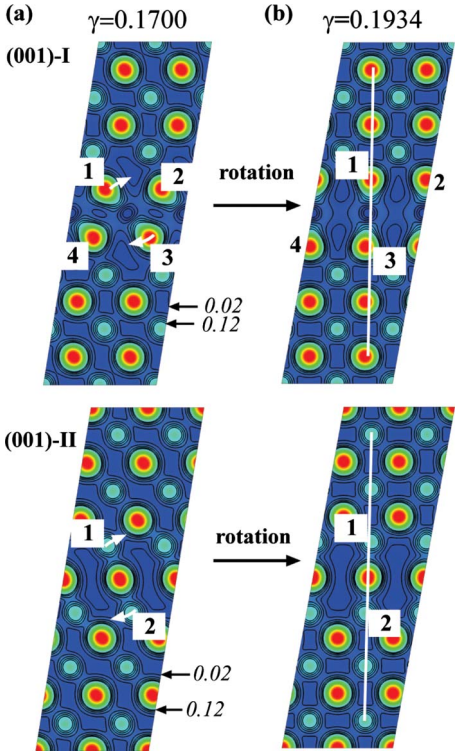

FIG. 12. (Color online) The changes in valence charge density of TiN(110)/1 ML-SiN/(110)TiN interface upon shear applied in the $[1\bar{1}0]$ direction just (a) before (strain γ=0.1700) and (b) after (strain γ=0.1934) instability. The white arrow shows the rotation of the Ti-N and Si-N bonds due to the shear. The small (black) italic numbers indicate the contours of the VCD.

can be reached only after a full one-atomic shear step corresponding to a shear strain equal to 1.0. This "rotational bond shear" explains in a natural way why in the $(111)[1\bar{1}0]$ slip system the instability occurs at the lower shear stress than the maximum ideal shear strength, because in all other slip systems the shear occurs under bond rearrangement and breaking as illustrated for the (111) interface in Fig. 4 of Ref. 57 and for the (110)[001] slip system below.

Figure 13 shows the changes in the VCD distribution of TiN(110)/1 ML-SiN/(110)TiN interface upon shear applied in the [001] direction just (a) before (strain γ=0.4242) and (b) after (strain γ=0.4526) the instability (c.f. Fig. 8). There is only a small distortion of the atomic arrangement just before the instability at a strain γ=0.4242 in both planes $(1\bar{1}0)$-I and $(1\bar{1}0)$-II [see Fig. 13(a), left]. After the instability at a strain γ=0.4526 there is clearly Ti-N bond breaking as marked by the double-arrows in Fig. 13(b), whereas the other neighbor Ti-N distance (e.g., between Ti-atom 1 and N-atom 3) decreases by about 15% as compared with that before the instability. One can also see the decrease in VCD in regions of the long Ti-N distance as well as in planes parallel next to the SiN interface. Thus, the zero-stress state at shear strain of $\leq$0.5 corresponds to a metastable intermediate which will shear easily to complete the one-atomic shear step.

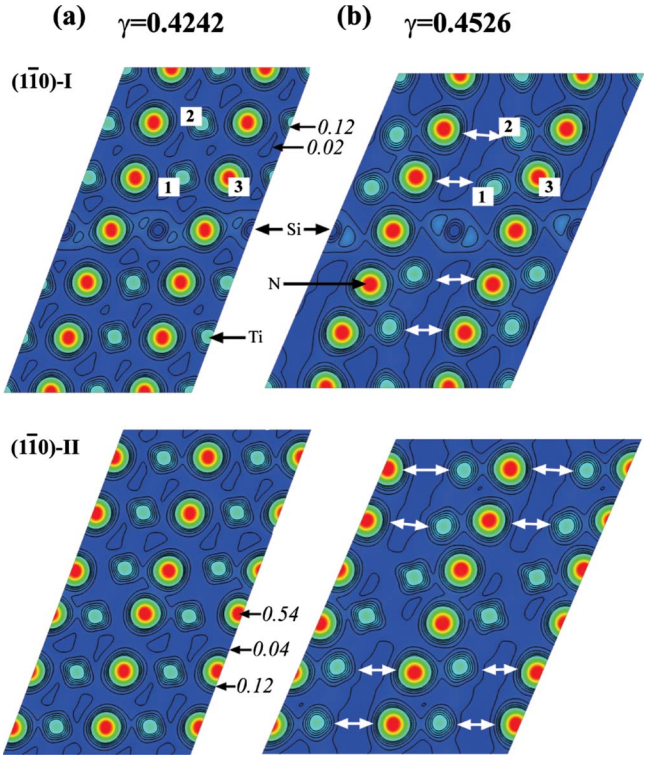

FIG. 13. (Color online) The changes in valence charge density of TiN(110)/1 ML-SiN/(110)TiN interface upon shear applied in the [001] direction just (a) before (strain γ=0.4242) and (b) after (strain γ=0.4526) the instability. The small (black) italic numbers indicate the contours of the VCD.

IV. DISCUSSION

The present results show that the strengthening of the SiN interfaces between TiN nanocrystals is due to valence charge transfer to that interface with formation of strong Si-N bonds. This behavior is similar to that already described for the stoichiometric, semicoherent TiN-(111)/Si_3N_4−(10$\bar{1}$0) interface by Hao *et al.*[30,31] In the present paper we have shown that this charge perturbation leads to Friedel oscillations and weakening of the bonds between the Ti and N atoms attached to the Si atoms within the interface. In the case of the (111) interface which contains only Si atoms, the Friedel oscillations are "in phase" so that the Ti-N bonds attached directly to the SiN interface are the "weakest link" where the decohesion and shear occur under the applied tensile and shear stresses (see Ref. 57 for further details). Because the (001) and (110) SiN interfaces contain both Si and N atoms, Friedel oscillations in the perpendicular planes containing either only Si or only N atoms within the interface are "phase shifted" with respect to each other, resulting in corresponding shifts of the weakest Ti-N bonds. As a result, the details of decohesion and ideal shear are much more complex. Nevertheless, they explain in a simple manner why the (110)[001] slip system is the strongest one because the critical shear instability involves TiN bond breaking which extends into the interior of the TiN slab (or nanocrystal).

Of course, all the semicoherent or pseudomorphic, distorted SiN_x interfaces considered by Hao *et al.* as well as in the present paper are special interfaces and not likely to occur solely in the nanocomposites with randomly oriented, 3–4 nm size grains, and where portions of the singular TiN crystalline surfaces are likely to extend no more than 1–2 nm^2. The experimentally found fact that the preferential (220) orientation of pure TiN films changed to random upon addition of SiN_x, when the maximum hardness has been achieved with about 1 ML of Si_3N_4 (Ref. 62) indicates that there is a strong driving force that minimizes the total interfacial energy by selecting the most stable and most frequently encountered interfaces, such as TiN-(111)/Si_3N_4−(10$\bar{1}$0) one[30] or some pseudomorphic substoichiometric SiN_x variety. It must be kept in mind that TiN nanocrystals of an almost regular shape[12] are terminated by a variety of possible lattice planes that are not accessible to a direct observation even in HRTEM because of the random orientation of the nanocrystals. Last but not least, since amorphous covalent solids can be prepared with a very low density of defects (see e.g., Ref. 63), incoherent interfaces with a low density of flaws may also occur.

The random orientation of the nanocrystals in the fully segregated nanocomposites with high thermal stability is important for their higher hardness as compared to heterostructures. This is because in the latter plasticity results from conventional crystallographic slip processes (which is, compared with bulk TiN, somewhat hindered by the Koehler mechanism[64]) while in the polycrystalline nanocomposites the crystalline grains are too small to deform by crystal plasticity and nearly all plastic straining occurs by shear at randomly oriented TiN/1 ML-SiN_x/TiN interfaces in the solid. In the present paper we demonstrated that this shear occurs in the stretched Ti-N bonds near the SiN_x interface as a result of the modulation of VCD caused by the Friedel oscillations.

Noting this new insight we can now recall the important developments in our earlier paper.[32] There we used the calculated shear strengths of the TiN/1 ML-SiN_x/TiN interfaces. Then, considering augmentation of these resistances by a pressure effect, deriving from these a tensile plastic resistance through invoking the polycrystalline Sachs[65] average, and finally considering the well-known Tabor factor relating the tensile plastic resistance to indentation hardness, we demonstrated that these considerations fully account for the measured hardnesses of the quasiternary nanocomposites of nc-TiN/a-Si_3N_4/$TiSi_2$ at a level in excess of 100 GPa. The validity of the Tabor factor for the ultrahard nanocomposites, which have a higher ratio of hardness to Young's modulus than diamond, has been recently verified[66] by means of nonlinear finite element modeling that accounts for pressure enhancement of elastic moduli and of flow stress.[67] We recall here also that a necessary condition for achieving such high hardnesses in fully segregated nanostructures requires a very low impurity content of less than 100 ppm[3,8] in order to form an almost flaw-free SiN_x interface.[9,10]

The finding of the present paper that, as a result of Friedel oscillations, the TiN bonds next to the strengthened SiN_x interface weaken, motivates a search for other TmN/SiN_x systems where such a weakening may occur to a lesser extent yet strengthening of the SiN_x interface is retained. However, it may turn out that Friedel oscillations with all their conse-

quences may impose a fundamental limit to the achievable hardness in nanocomposites to be in the range of $\leq$150 GPa.[32]

It is worth noting that the observed form of shear adjacent to the {111} interfaces of being made up of two complementary ⟨112⟩ type half steps in the {111} plane,[57] demonstrating very similar features characteristic of fcc metal crystals, may suggest that this might be more universal in all TiN crystallites with glide of extended dislocations containing stacking faults between partials, etc.[68] (see also Ref. 69). However, this will remain as an interesting conjecture until demonstrated to be so. Furthermore, the phase shift of the Friedel oscillations observed for the (001) and (110) interfaces resulting in very complex atomistic mechanisms of decohesion and shear should be important also in other TmN-SiN_x nanocomposite systems.

V. CONCLUSIONS

Using *ab initio* DFT method we calculated decohesion and shear strengths of several fcc-TiN/1 ML-SiN/TiN interfaces. The strengthening by a factor of 4–10 reported in our earlier paper[32] is due to valence charge transfer to the 1 ML-SiN interface which strengthens the Si-N bonds. The Friedel oscillations, which occur as a consequence of the electronic perturbation of the system, result in a weakening of the Ti-N bonds within TiN planes attached to the 1 ML-SiN interface. These are the weakest links where decohesion and shear occur under applied normal or shear stress. In spite of this weakening, the overall strengthening of the interface provides the fcc-TiN/1 ML-SiN/TiN heterostructures with hardness enhancement up to about 35 GPa. In the nc-TiN/a-Si_3N_4 nanocomposites with randomly oriented TiN nanocrystals, the Sachs's averaging, together with the pressure enhancement of flow stress and Tabor's relationship (whose validity for these materials has been verified) explain in an easily understandable manner that hardness in excess of 100 GPa can be achieved in such nanocomposites.

ACKNOWLEDGMENTS

This work has been supported by the German Research Foundation (DFG), and by the European Commission within the project NoE EXCELL, Contract No. 5157032. The research of A.S.A. at MIT was supported by the Department of Mechanical Engineering at M.I.T.

*Corresponding author. FAX: +49 89 289 13626; veprek@lrz.tum.de

[1] S. Veprek and S. Reiprich, Thin Solid Films **268**, 64 (1995).
[2] S. Veprek, J. Vac. Sci. Technol. A **17**, 2401 (1999).
[3] S. Veprek, M. G. J. Veprek-Heijman, P. Karvankova, and J. Prochazka, Thin Solid Films **476**, 1 (2005).
[4] S. Veprek and M. G. J. Veprek-Heijman, Surf. Coat. Technol. **202**, 5063 (2008).
[5] "nc" stands for nanocrystalline, "a" for x-ray amorphous, and the stoichiometry Si_3N_4 is used to emphasize that the binding energy of the Si 2*p* electrons of the interfacial monolayer is the same as in stoichiometric, bulk silicon nitride.
[6] The crystal structure of TiN is of NaCl type and consists of two interpenetrating fcc lattices of Ti and N. Because of the close correspondence of the NaCl structure and fcc lattices with regard to crystallographic symmetry and slip characteristics we treat TiN as if it was fcc, except when we discuss in detail the ideal shear responses, where recognition of the differences in the two structures is essential.
[7] S. Veprek, H. D. Männling, P. Karvankova, and J. Prochazka, Surf. Coat. Technol. **200**, 3876 (2006).
[8] S. Veprek, P. Karvankova, and M. G. J. Veprek-Heijman, J. Vac. Sci. Technol. B **23**, L17 (2005).
[9] A. S. Argon and S. Veprek, Mater. Res. Soc. Symp. Proc. **697**, 3 (2002).
[10] S. Veprek and A. S. Argon, J. Vac. Sci. Technol. B **20**, 650 (2002).
[11] S. Veprek, S. Mukherjee, P. Karvankova, H.-D. Männling, J. L. He, K. Moto, J. Prochazka, and A. S. Argon, J. Vac. Sci. Technol. A **21**, 532 (2003).
[12] S. Christiansen, M. Albrecht, P. Strunk, and S. Veprek, J. Vac. Sci. Technol. B **16**, 19 (1998).
[13] H. Söderberg, M. Odén, J. M. Molina-Aldareguia, and L. Hultman, J. Appl. Phys. **97**, 114327 (2005).
[14] H. Söderberg, J. M. Molina-Aldareguia, T. Larrsson, L. Hultman, and M. Odén, Appl. Phys. Lett. **88**, 191902 (2006); H. Söderberg, M. Odén, A. Flink, J. Birch, P. O. A. Persson, M. Beckers, and L. Hultman, J. Mater. Res. **22**, 3255 (2007).
[15] X. Hu, H. Zhang, J. Dai, G. Li, and M. Gu, J. Vac. Sci. Technol. A **23**, 114 (2005).
[16] L. Hultman, J. Bareno, A. Flink, H. Söderberg, K. Larsson, V. Petrova, M. Odén, J. E. Greene, and I. Petrov, Phys. Rev. B **75**, 155437 (2007).
[17] M. Kong, W. Zhao, L. Wie, and G. Li, J. Phys. D **40**, 2858 (2007).
[18] S. Z. Li, Q. F. Fang, Q. Liu, Z. S. Li, J. Gao, P. Nesladek, J. Prochazka, M. G. J. Veprek-Heijman, and S. Veprek, Compos. Sci. Technol. **65**, 735 (2005).
[19] X. Hu, Z. Han, G. Li, and M. Gu, J. Vac. Sci. Technol. A **20**, 1921 (2002).
[20] S. Veprek, M. Haussmann, and S. Reiprich, J. Vac. Sci. Technol. A **14**, 46 (1996).
[21] J. Prochazka, P. Karvankova, M. J. G. Veprek-Heijman, and S. Veprek, Mater. Sci. Eng., A **384**, 102 (2004).
[22] S. Veprek, H.-D. Männling, P. Holubar, and M. Jilek, Mater. Sci. Eng., A **366**, 202 (2004).
[23] R. F. Zhang, S. H. Sheng, and S. Veprek, Appl. Phys. Lett. **90**, 191903 (2007).
[24] B. Alling, E. I. Isaev, A. Flink, L. Hultman, and I. A. Abrikosov, Phys. Rev. B **78**, 132103 (2008).
[25] R. F. Zhang and S. Veprek, Mater. Sci. Eng., A **424**, 128 (2006).
[26] R. F. Zhang and S. Veprek, Thin Solid Films **516**, 2264 (2008).
[27] R. F. Zhang and S. Veprek, Phys. Rev. B **76**, 174105 (2007).
[28] Even at the conditions of low nitrogen activity, the Gibbs free energy of the reaction $4SiN = Si_3N_4 + Si$ is −136 kJ/mol atom.

[29] S. Veprek and M. G. J. Veprek-Heijman, Surf. Coat. Technol. **201**, 6064 (2007).
[30] S. Hao, B. Delley, S. Veprek, and C. Stampfl, Phys. Rev. Lett. **97**, 086102 (2006).
[31] S. Hao, B. Delley, and C. Stampfl, Phys. Rev. B **74**, 035402 (2006).
[32] S. Veprek, A. S. Argon, and R. F. Zhang, Philos. Mag. Lett. **87**, 955 (2007).
[33] X. Liu, B. Gottwald, C. Wang, Y. Jia, and E. Westkämper, in *High Performance Computing in Science and Engineering '07*, edited by W. E. Nagel (Springer Verlag, Berlin, Heidelberg, 2008), pp. 117–136.
[34] G. Kresse and J. Hafner, Phys. Rev. B **47**, 558 (1993); **49**, 14251 (1994).
[35] G. Kresse and J. Furthmüller, Comput. Mater. Sci. **6**, 15 (1996).
[36] G. Kresse and J. Furthmüller, Phys. Rev. B **54**, 11169 (1996).
[37] G. Kresse and D. Joubert, Phys. Rev. B **59**, 1758 (1999).
[38] J. P. Perdew and Y. Wang, Phys. Rev. B **45**, 13244 (1992).
[39] H. J. Monkhorst and J. D. Pack, Phys. Rev. B **13**, 5188 (1976).
[40] D. Roundy, C. R. Krenn, M. L. Cohen, and J. W. Morris, Jr., Phys. Rev. Lett. **82**, 2713 (1999).
[41] D. Roundy, C. R. Krenn, M. L. Cohen, and J. W. Morris, Jr., Philos. Mag. A **81**, 1725 (2001).
[42] F. D. Murnaghan, Proc. Natl. Acad. Sci. U.S.A. **30**, 244 (1944).
[43] F. Birch, Phys. Rev. **71**, 809 (1947); J. Geophys. Res. **83**, 1257 (1978).
[44] P. Vinet, J. Ferrante, J. R. Smith, and J. H. Rose, J. Phys. C **19**, L467 (1986).
[45] J. H. Rose, J. R. Smith, F. Guinea, and J. Ferrante, Phys. Rev. B **29**, 2963 (1984).
[46] K. Köllisch and W. Schnick, Angew. Chem. **111**, 368 (1999).
[47] A. Zerr, R. Riedel, T. Sekine, J. E. Lowther, W.-Y. Ching, and I. Tanaka, Adv. Mater. **18**, 2933 (2006).
[48] E. Horvath-Bordon, R. Riedel, A. Zerr, P. F. McMillan, G. Auffermann, Y. Prots, W. Bronger, R. Kniep, and P. Kroll, Chem. Soc. Rev. **35**, 987 (2006).
[49] H. Kwart and K. G. King, *d-Orbitals in the Chemistry of Silicon, Phosphorus and Sulfur* (Springer-Verlag, Berlin, 1977).
[50] H. Schmidbaur, in *Tailor-made Silicon-Oxygen Compounds*, edited by R. Corriu and P. Jutzi (Friedrich Vieweg and Sons, Göttingen, 1996), p. 13.
[51] A. R. West, *Solid State Chemistry and its Applications* (John Wiley and Sons, Chichester, 1984).
[52] J. Friedel, Philos. Mag. **43**, 152 (1952); Adv. Phys. **3**, 446 (1954).
[53] W. A. Harrison, *Electronic Structure and Properties of Solids* (W. H. Freeman and Co., San Francisco, 1980).
[54] E. Roduner, *Nanoscopic Materials* (RSC Publishing, Royal Soc. of Chem., Cambridge, 2006).
[55] N. N. Greenwood and A. Earnshaw, *Chemistry of Elements* (Pergamon, Oxford, 1984). [Quoted after the German translation *Chemie der Elemente*, 2nd ed. (VCH Verlagsgesellschaft, Weinheim, 1990).]
[56] S. Hao, private communication.
[57] R. F. Zhang, A. S. Argon, and S. Veprek, Phys. Rev. Lett. **102**, 015503 (2009).
[58] It is essential to point out that in Fig. 5 while all strains in the abscissa are labeled as strain, they differ fundamentally where in the decohesion case the strains are normal strains while in the ideal shear case they are shear strains. Moreover, for both cases strains are represented there as averages over the entire simulation cell, i.e., the border displacements divided by the height of the simulation cell. While in the decohesion case no serious ambiguity arises, there is an essential clarification necessary for the shear cases. There, after the peak resistance the shear strain concentrates into the interatomic space where the actual shear occurs, while the rest of the cell elastically unloads as is clear from the abrupt drop in the stress. Thus, the actual system ideal shear strains are not just the residual strains shown at zero shear stress in the figure which are attenuated by the ratio of the interplanar spacing where the shear occurs to the cell height. The actual system ideal shear strains are much larger by the reciprocal of this attenuation factor. For example, the actual system ideal shear strains are: $\gamma_i = 1.41$ for the (001)[110]; and $\gamma_i = 2.00$ for the (001)[100] systems, respectively. Similar considerations also hold for the ideal shear results shown in Fig. 8.
[59] J. Frenkel, Z. Phys. **37**, 572 (1926).
[60] R. W. Hertzberg, *Deformation and Fracture Mechanics of Engineering Materials*, 3rd ed. (John Wiley and Sons, New York, 1989).
[61] Note that the considerations discussed above in the remark in connection with Fig. 5 also apply here.
[62] A. Niederhofer, P. Nesladek, H.-D. Männling, K. Moto, S. Veprek, and M. Jilek, Surf. Coat. Technol. **120-121**, 173 (1999).
[63] X. Liu, B. E. White, Jr., R. O. Pohl, E. Iwanizcko, K. M. Jones, A. H. Mahan, B. N. Nelson, R. S. Crandall, and S. Veprek, Phys. Rev. Lett. **78**, 4418 (1997).
[64] J. S. Koehler, Phys. Rev. B **2**, 547 (1970).
[65] G. Sachs, Z. Ver. Dtsch. Ing. **72**, 734 (1928).
[66] M. G. J. Veprek-Heijman, R. G. Veprek, A. S. Argon, D. M. Parks, and S. Veprek, Surf. Coat. Technol. **203**, 3385 (2009).
[67] R. G. Veprek, D. M. Parks, A. S. Argon, and S. Veprek, Mater. Sci. Eng., A **448**, 366 (2007).
[68] A. S. Argon, *Strengthening Mechanisms in Crystal Plasticity* (Oxford University Press, Oxford, 2008).
[69] V. Vitek, Philos. Mag. **18**, 773 (1968).